Doping the permanent magnet CeFe11Ti with Co and Ni using ab-initio density functional methods

Doping the permanent magnet $CeFe_{11}Ti$ with Co and Ni using ab-initio density functional methods

A Dasmahapatra[1], R Martinez-Casado[2] , C Romero-Muñiz[3], M F Sgroi[4], A M Ferrari[1,5] and L Maschio[1,5]

[1] University of Torino, Dipartimento di Chimica, via P. Giuria 5, I-10125 Turin, Italy

[2] Department of Materials Physics, Faculty of Physical Sciences, University Complutense Madrid, 28040, Madrid, Spain

[3] Department of Physical, Chemical and Natural Systems, Universidad Pablo de Olavide, Ctra. Utrera Km. 1, E-41013, Seville, Spain

[4] Centro Ricerche FIAT, Strada Torino 50, 10043 Orbassano (TO), Italy

[5] NIS (Nanostructured Interfaces and Surfaces) Centre of Excellence, University of Turin, Italy

Abstract:

High performance magnets are valuable in the light of the modern energy crunch in the world primarily because of their applicability in electric motor vehicles. We study two compounds: $CeCoFe_{10}Ti$ and $CeNiFe_{10}Ti$ using hybrid density functional computations. Our aim is to observe effects of adding Co and Ni to the parent compound $CeFe_{11}Ti$, which is a well-known permanent magnet. Using a solid solution algorithm in the ab-initio CRYSTAL code, we determine 16 symmetrically distinct ways in which Ni or Co can be added. These 32 configurations (16 for each Co and Ni) are then further analyzed for their total energies, spin configurations, partial density of states (PDOS) and magnetic anisotropic energies (MAE). Our work shows that addition of Co slightly enhances magnetic properties. The addition of Ni weakens the hybridization between Ce-f and Fe-d orbitals and leads to a decrease in saturation magnetic values and MAE.

1. Introduction:

Rare Earth Elements (REE) have been identified as a key element in permanent magnets for the past three decades. [1,2,3] These RE-Fe intermetallic compounds are also important for electric vehicle (EV) motor and wind generators. [4,5] However due to limited availability and price of the rare earth metals, research interest still sustains in these materials. In particular, computational studies are becoming increasingly important as they can provide atomistic modeling and establish links between chemical composition, interaction of the magnetic spins and finally lead to the proposition of novel magnetic materials.[6,7,8,9] While one popular field of research is the computational screening using structure-prediction algorithms to predict new magnets,[10,11] other studies focus on substitution of an element in RE-Fe based magnets to enhance magnetic properties.[12,13,14]

In a previous publication[15] we used periodic hybrid-exchange density functional theory (DFT) calculations as implemented in the CRYSTAL code [16] to systematically study the electronic structure of a prospective permanent magnet candidate, $CeFe_{11}Ti$. We analyzed the spin configuration and observe a ferromagnetic coupling among the Fe atoms. The neighboring atoms Ce and Ti are however in an opposite spin down configuration and thus the overall spin of the compound is classified as ferrimagnetic. Our calculations also suggested that the Ce atom is trivalent. In addition, we established that the valence electron in Ce is not iterant and is located in the 4f orbital. However, we did not implement the Hubbard I approximation as in Locht et al. [17] and thus refrain from classifying this electron as localized. With the [0 0 1] crystallographic axis as an easy axis we computed the MAE (K_1) along this direction as 1.67 meV $f.u.^{-1}$ (1.57 MJ m^{-3}).

In this paper, we extend our previous work by studying two derivatives of $CeFe_{11}Ti$ with Co and Ni added in small amounts: $CeCoFe_{10}Ti$ and $CeNiFe_{10}Ti$. The substitution with Co and Ni is an approach that has been discussed in previous work. [18,19,20] This is a prevalent way to enhance the Curie temperature (T_c) and saturation magnetization (M_s) in these class of compounds. Our primary focus in this work is to systematically add the dopants – Co and Ni and observe the effects on the properties of the parent material through the analysis of all the possible crystallographic structures with equivalent stoichiometry. In addition, substitution of Fe atoms by Ni or Co shifts the Curie temperature to higher values, as it is observed in similar compounds like $La(Fe,Si)_{13}$-based magnetic refrigerants. [21]

In the following section, we discuss the computational methods adopted for this work. In the Results and Discussion part, we first take a look at the ways Co and Ni can be added to $CeFe_{11}Ti$. We select 3 energetically favorable configurations for each Co and Ni. This is followed by with an analysis of the partial Density of States (PDOS) and estimation of magnetic anisotropic energy (MAE) for these selected configurations.

2. Computational Details:

The computational work in this paper has been carried out with two separate methods – all electron(AE) calculations using the CRYSTAL code [22]and plane-wave(PW) calculations using the VASP code. [23,24,25,26] AE calculations are used to 1) determine probable configurations, 2) optimize cell and atom coordinates and 3) analyze partial density of states for the doped models of Ce-Ti-Fe permanent magnets whereas PW calculations are used to compute magnetocrystalline anisotropy energy for selected models.

The CRYSTAL code relies on the Linear combination of atomic orbitals (LCAO) approach where crystalline orbitals are expressed by a basis set of atom-centered Gaussian orbitals. Consistent with our previous work, we use spin-polarized density functional theory and PBE functional with 10% Hatree-Fock exchange (PBE10). [27,28] Regarding the basis sets, for Ce, Ti and Fe we use the one labeled as BS2 in ref. [15], while for Co we used a basis-set of hierarchy s(842111) p(6311) d(411) f(11) and for Ni we used the same basis-set as in [29].

Starting from the parent $CeFe_{11}Ti$, we exploited a solid-solution algorithm (discussed in detail later) and obtained 16 different configurations for each of the Co and Ni atom doping. An important part of our work was to optimize all these crystal structures for both cell and atom positions. Structures were optimized using the Broyden–Fletcher–Goldfarb–Shanno scheme of Hessian updating. [30,31] Default convergence criteria, as in [15] were adopted for both gradient and nuclear displacements. The self-consistent field (SCF) algorithm energy threshold was set to 10^{-8} Hartree. Furthermore, for subsequent SCF cycles, direct inversion of the iterative subspace (DIIS) convergence accelerator was used, with an energy threshold for activation set to 10^{-2} Ha. [32] Integration over reciprocal space was carried out using Monkhorst-Pack (MP) meshes of 8x8x8 and the Coulomb and exchange series (computed in direct space) was truncated at thresholds of [10, 10, 10, 20, 40].[33] The total energy of the structures presented in this work is only obtained after several cycles of these stringent optimization criteria. However, implementation of spin-orbit coupling (SOC) and non-collinear spins are a limitation of the CRYSTAL package and hence we turn to PW calculations to estimate the magnetocrystalline anisotropy energy (MAE).

We performed MAE computations for select structures of the doped Ce-Fe-Ti magnet using the force theorem approach [34,35] as implemented in VASP . We used the Projector Augmented Wave (PAW) pseudo-potentials and Generalized Gradient Approximation (PBE-GGA) of electron exchange and correlation. [27,36,37] We chose a high cut-off energy of 600 eV in accordance with the computations for the parent compound. All structures were re-optimized using a conjugate gradient algorithm until forces on atoms were less than 0.01 eV/A and allowing relaxation of the cell volume as well. The Vosko–Wilk–Nusair interpolation[38] was then used to implement spin polarization. Under this approximation, it is assumed that MAE arises from spin–orbit coupling, which is treated as a perturbation of the scalar relativistic Hamiltonian used in standard DFT. Thus, there are two steps to compute the MAE: 1) A collinear calculation was carried out in order to determine the correct magnetic ground state. 2) Non-collinear calculations were performed with the obtained geometry and the magnetic configuration from step 1 with spin–orbit coupling. Crystallographic directions chosen were [0 0 1], [1 1 0], [1 0 0] and [0 1 0] along which non self-consistent calculations were preformed to determine the total magnetic moment. The difference in total energy between two such spin non-collinear configurations is the direct measure for MAE.

3. Results and Discussions:

3.1. Structural models

- $CeFe_{11}Ti$:

The pure compound $CeFe_{11}Ti$ has $ThMn_{12}$-type body-center-tetragonal crystal structure with space group I4/mmm(group number 139). The Ce atoms are located at the 2a (4/mmm) sites, while Fe and Ti are in 3 separate sub-lattices - 8i (m2m), 8j (m2m), and 8f (2/m). The role of the Ti atoms is to stabilize the structure as discussed in [15] and always prefer to occupy the 8i sites.

Spin configuration analysis showed that $CeFe_{11}Ti$ energetically prefers the ferrimagnetic configuration with all Fe in spin up and Ce and Ti atoms in spin down in the unit cell. The valence electron in our computations is non-itinerant and primarily located in the 4f orbital.

It is to be mentioned here that for all our crystal structures, there is a slight disparity between the a and b lattice parameters. The use of periodic boundary conditions in DFT calculations do not allow for a true random distribution of Ti/Fe atoms in the 8i sites. Thus, there exists, a slight asymmetry between the [100] and [010] crystallographic directions. We, also, do not impose any restriction in the lattice parameters during the geometrical minimization and thus this artifact arises due to lack of perfectly disordered distribution of Ti/Fe in 8i sites.

- $CeCoFe_{10}Ti$ and $CeNiFe_{10}Ti$:

The conventional unit cell of $CeFe_{11}Ti$ has 26 atoms with 2 formula units. As expected, 2 8i sites are now occupied by Ti atoms. While modeling the derivative compounds with additional Co and Ni, we started from this configuration with the aim to substitute 2 Fe atoms with Co or Ni. However, the structural details of the doped structure are to be determined.

The solid solution algorithm implemented in the CRYSTAL code, [39,40] ensures that for any substitution fraction x, the program finds the total number of atomic configurations possible and determines the symmetry-irreducible configurations among them. Symmetry irreducible configurations can, then, be optimized and further probed for properties. A full discussion of the underlying mathematics of this algorithm is beyond the scope of this paper. We turn the attention of the reader to References [39] and [40] for further details of this algorithm. Starting from $CeFe_{11}Ti$, the algorithm predicted 16 symmetrically irreducible configurations where Co/Ni atoms occupied unique positions. Co and Ni atoms prefer to substitute Fe atoms in 8j and 8f sites. For the scope of this paper, we will refer to the Fe's as their atom number (ranging from 3 to 24 out of 26 total atoms in the system) instead of the symmetry of the occupied sites. A representative model is shown in Figure 1 where the substitution of Fe has been highlighted. Spin configurational analysis (not discussed in detail here) shows that Co and Ni atoms prefer to be spin-up always, aligned with the Fe atoms. If the spin-down configuration (opposite to the

spin of the Fe atoms) is enforced, an energy difference of +0.17 eV and +0.42 eV occurs for the Co and Ni atom, respectively.

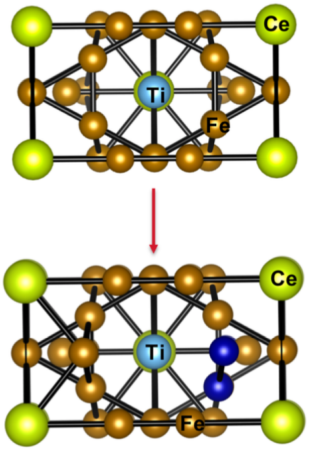

Figure 1: Representative conventional unit cell for the crystal structures of $CeFe_{11}Ti$ and $CeCoFe_{10}Ti$. Green spheres are representative of Ce atoms, Fe atoms are brown spheres, Ti is light blue and Co atoms are indicated by dark blues spheres. Since we consider conventional cell of 26 atoms, 2 Fe atoms can be substituted by Co. The structure is aligned along the c-axis.

Figure 2 shows the formation energies per unit cell for each of these 16 configurations (Ni, on the left and Co, on the right) after suitable geometry optimization. The formation energy of $CeCoFe_{10}Ti$ is defined in equation (1) as:

$$E_f = E(CeCoFe_{10}Ti) - E(Ce) - 10E(Fe) - E(Ti) - E(Co) \quad \text{(Equation 1)}$$

where $E(CeCoFe_{10}Ti)$, $E(Ce)$, $E(Fe)$, and $E(Ti)$, are the energies of $CeCoFe_{10}Ti$, Ce, Fe, Ti and Co respectively. Isolated atoms for Ce, Ti, Ni and Co have been surrounded by 'ghost' atoms up to 6˚A in order to compensate for basis set superposition error (BSSE) effects. The reference energies are thus computed as: $E(Fe) = -3.44\times10^4$ eV/unit cell, $E(Ce) = -1.29\times10^4$ eV/unit cell, $E(Ti) = -2.31\times10^4$ eV/unit cell, $E(Co) = -3.76\times10^4$ eV/unit cell and $E(Ni) = -4.10\times10^4$ eV/unit cell. While some configurations are only minutely different in energy than the others, for simplicity we selected 3 representatives among the lowest formation energy configurations for

the remainder of the computations. In a real sample, we expect all of these configurations to coexist, in variable proportions according to the temperature and fabrication process.

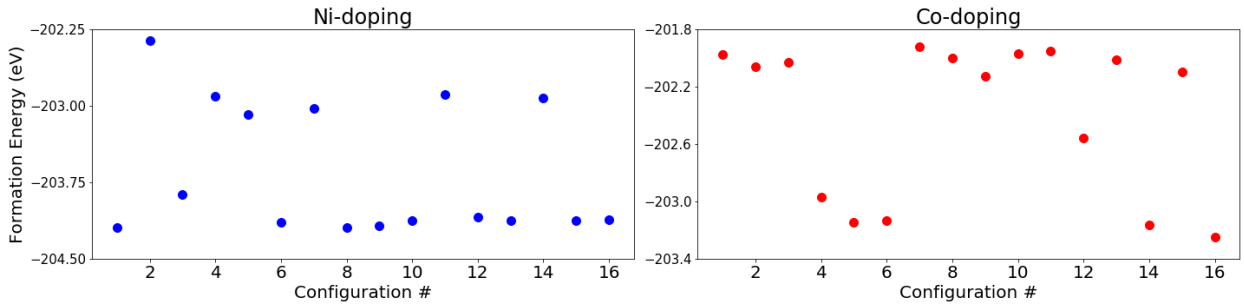

Figure 2: Formation energies per unit cell for each of the 16 configurations for Ni-doped (left) and Co-doped(right) compounds as defined in equation 1. The best models (in terms of lowest formation energy) are configurations 1, 8 and 9 for Ni and 5, 14 and 16 for Co.

The lattice parameters for the lowest energy model of $CeCoFe_{10}Ti$ and $CeNiFe_{10}Ti$ are listed in Table 1. We observe only a minor effect of Co/Ni substitutions on the lattice vectors a, b and c with respect to the parent compound. We can compare our results to the work of Yang et al, who studied the effect of substitution of Ni to $YTi(Fe_{1-x}Ni_x)_{11}$ magnets, where the addition of Ni is seen to decreases the lattice constant a by 0.70% while having no effect on c.[19] At comparable mole-fractions (0.08, 2 out of 26 atoms of Fe is replaced by Ni/Co), between 3 different configurations, our results do not show a unanimous trend. While for configuration 1 in Ni substitution all a, b and c constants stay same, for configuration 8, a and b decrease by ~0.3%. In case of substitution by Co, the trends are regular. For all three configurations, a and b increases while c remains constant. Distances between doped Ni and Co atoms and their nearest neighboring Fe atoms range between 2.3 – 2.6 Å.

Configuration #	**a(Å)**	**b(Å)**	**c(Å)**	**M_S(μB f.u. $^{-1}$)***
$CeFe_{11}Ti$	8.33	8.28	4.66	24.04
$CeNiFe_{10}Ti$				
1	8.35	8.26	4.67	22.78
8	8.31	8.28	4.64	22.58
9	8.34	8.29	4.66	22.77

$CeCoFe_{10}Ti$				
5	8.27	8.31	4.65	23.59
14	8.24	8.31	4.66	23.58
16	8.26	8.30	4.64	23.34

Table 1: Comparison of lattice constants for the parent material and the Co/Ni substituted compounds. The saturation magnetization values are computed within CRYSTAL using the hybrid PBE10 functional. Note that the slight difference between a and b parameters is an artifact of periodic boundary conditions in our computations.

3.2. Analysis of partial Density of States (p-DOS):

Figure 3 shows the scalar relativistic partial density of states (PDOS) projected on individual elements in $CeCoFe_{10}Ti$ and $CeNiFe_{10}Ti$. The addition of Ni or Co do not have any significant effect and the PDOS is composed mainly of Fe-d orbitals. In addition, a strong hybridization between Fe-d and Ce-f orbitals is observed in the form of a peak at ~1.5 eV in the conduction band. This strong hybridization is also believed to affect the magnetic properties of the compound. While the addition of Co, slightly increases this peak, the addition of Ni seems to dampen it, leading to lower saturation magnetization (M_S) values of the Ni-doped compound.

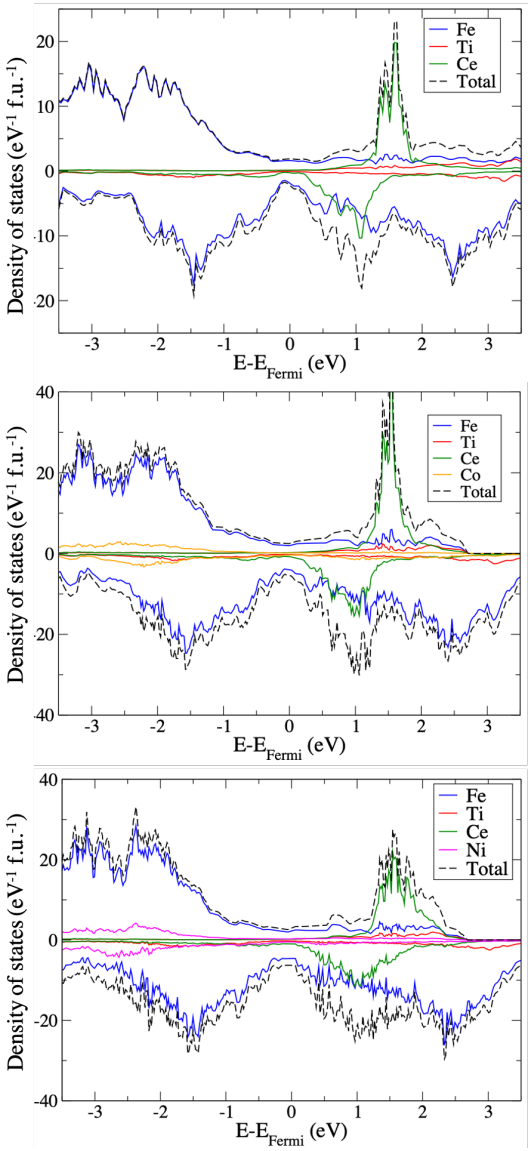

Figure 3: Representative projected DOS for the lowest energy configuration of $CeCoFe_{10}Ti$ (middle) and $CeNiFe_{10}Ti$ (bottom) as computed using PBE10 hybrid functional. For clarity in comparison, we also include the PDOS of the parent compound $CeFe_{11}Ti$ (top). For $CeCoFe_{10}Ti$ and $CeNiFe_{10}Ti$, the Fe PDOS is averaged over the 10 atoms in the unit cell. For all plots, the black line represents the total DOS, while the blue, red, and green solid lines describe the projected one on the Fe, Ti, and Ce atoms, respectively. Orange line is used to represent Co and purple line for Ni in each of the doped compounds.

The magnetic moment per atom and l-decomposed number of electrons for the $CeCoFe_{10}Ti$ (in μB) and $CeNiFe_{10}Ti$ (see Table 2) clarifies that similar to the parent compound, electrons are mainly located in d-orbitals for Fe, Co/Ni and Ti and f-orbitals for Ce.

$CeCoFe_{10}Ti$	**sp**	**d**	**f**	**total**
Fe (i)	-0.17	2.71	0	2.54
Fe (j)	-0.17	2.41	0	2.24
Fe (f)	-0.19	2.86	0	2.67
Ce	-0.15	-0.27	-0.68	-1.09
Ti	-0.14	-1.07	-0.04	-1.25
Co	-0.05	1.41	0	1.36
$CeNiFe_{10}Ti$	**sp**	**d**	**f**	**Total**
Fe (i)	-0.12	2.68	0.00	2.55
Fe (j)	-0.17	2.44	0.00	2.27
Fe (f)	-0.13	2.80	0.00	2.67
Ce	-0.13	-0.22	-0.86	-1.20
Ti	-0.15	-1.11	-0.05	-1.30
Ni	-0.19	0.79	0.00	0.61

Table 2: Magnetic moment per atom and l-decomposed number of electrons for $CeCoFe_{10}Ti$ and $CeNiFe_{10}Ti$ as computed in the CRYSTAL code using the hybrid PBE10 functional. The models used in the table are the lowest energy configuration for each compound.

3.3. Magnetic Anisotropy calculations

We now turn our attention to the computation of magnetocrystalline anisotropy of these doped compounds. As in our former work, the anisotropy constant is $K_1 = E_{110} – E_{001}$, where E_{110} and E_{001} are total energies when magnetization is aligned along the [1 1 0] and [0 0 1]

crystallographic axes. Since [1 0 0] and [0 0 1] directions have slight asymmetry as in the case for the pure compound, we use the [1 1 0] as the reference basal plane. Table 3 summarizes the MAE values.

It is interesting to note that no large differences can be observed between the MAE value for the chosen symmetry-irreducible configurations of the doped compounds. As seen from Table 3, Co-doped compounds, configurations 5 and 14 increase the MAE while configuration 16 decreases it as compared to the parent compound. For Ni, there is an artificial anisotropy between a and b crystallographic axes, that reflects a scattering of the MAE values between [1 0 0] and [0 1 0] directions. The direction [1 1 0] is still a reference to the xy plane since the total energy with spin-orbit coupling always lies in between. The values of MAE are further lower than the Co-doped compounds.

Magnetic hardness calculated as: $\kappa = \sqrt{\frac{K_1}{\mu_0 M_S^2}}$; where M_S is the saturation magnetization, $K_{1\ is}$ the magnetocrystalline anisotropy constant and μ_0 the vacuum permeability. κ is an important parameter to assess if a material is suitable for permanent magnets. The M_S computed from plane-wave calculations show that the Co-substituted compounds we have considered either satisfy $\kappa > 1$ or are very close to it, and thus qualify as good candidates for a possible permanent magnet. The same does not apply to Ni-substituted compounds, that appear to be less promising in this respect.

Configuration #	**MAE (MJm^{-3})**	**M_S(μB f.u. $^{-1}$) from VASP**	**κ**
$CeFe_{11}Ti$	1.67	20.04	1.01
$CeCoFe_{10}Ti$			
5	1.72	20.41	1.02
14	1.72	20.41	1.02
16	1.45	20.32	0.94
$CeNiFe_{10}Ti$			
1	1.27	19.71	0.91
8	1.15	19.89	0.85

9	1.29	19.90	0.90

Table 3: Magnetocrystalline anisotropy energy and magnetic hardness (κ) as obtained using pane-wave computations in VASP. The saturation magnetization values (M_S) used to calculate κ are also added.

4. Conclusions:

In this work we continue the computational design of novel permanent magnets (see reference [15]) with two new materials: $CeCoFe_{10}Ti$ and $CeNiFe_{10}Ti$. We use density functional theory and hybrid functionals (PBE + 10% HF exchange) as implemented in the CRYSTAL code. For the determination of magnetic properties, we rely on the use of the plane-wave VASP code using pseudo-potentials. The composition is derived by doping Co and Ni to the existing permanent magnet $CeFe_{11}Ti$. We start by substituting Fe atoms by Co/Ni. The tedious part of determining which Fe atoms to substitute is made possible by the use of the automated solid solution algorithm implemented in the CRYSTAL code. Using conventional unit cell for the parent system, the solid solution algorithm determined 16 symmetrically irreducible configurations in which Co or Ni atoms can be substituted for two Fe atoms in the parent material. We then computed the formation energies of these 32 unique configurations and identified 3 favorable configurations that had the lowest formation energies.

Further analysis was performed on these 3 configurations that included relativistic partial density of states, saturation magnetization and magnetic anisotropic energy. Our computations determined that while doping with Co preserved the magnetic properties of the parent material and even enhanced the magnetic hardness (κ) slightly, the addition of Ni has an opposite effect. Addition of Ni weakens the strong hybridization between Fe-d and Ce-f orbitals

that leads to lower M_S and MAE values. Thus, while future work can focus on varying the amount of Co in the material so to further enhance magnetic properties, the addition of Ni is not idealistic.

Data Availability:

The data that support the findings of this study are available from the corresponding author, AD and LM, upon reasonable request.

Acknowledgements:

We are grateful for the funding from the European Commission Horizon 2020 research and innovation program Novamag under grant 686116.

References:

(1) Sagawa, M.; Hiraga, K.; Yamamoto, H.; Matsuura, Y. Permanent Magnet Materials Based on the Rare Earth-Iron-Boron Tetragonal Compounds (Invited). *IEEE Trans. Magn.* **1984**. https://doi.org/10.1109/TMAG.1984.1063214.

(2) Kirchmayr, H. R. Permanent Magnets and Hard Magnetic Materials. *Journal of Physics D: Applied Physics*. 1996. https://doi.org/10.1088/0022-3727/29/11/007.

(3) Burzo, E. Permanent Magnets Based on R-Fe-B and R-Fe-C Alloys. *Reports Prog. Phys.* **1998**. https://doi.org/10.1088/0034-4885/61/9/001.

(4) McCallum, R. W.; Lewis, L.; Skomski, R.; Kramer, M. J.; Anderson, I. E. Practical Aspects of Modern and Future Permanent Magnets. *Annu. Rev. Mater. Res.* **2014**. https://doi.org/10.1146/annurev-matsci-070813-113457.

(5) Hanrahan, D.; Toffolo, D. Permanent-Magnet Generators. *IEEE Trans. Power Appar. Syst.* **2007**. https://doi.org/10.1109/tpas.1963.291399.

(6) Drebov, N.; Martinez-Limia, A.; Kunz, L.; Gola, A.; Shigematsu, T.; Eckl, T.; Gumbsch, P.; Elsässer, C. Ab Initio Screening Methodology Applied to the Search for New Permanent Magnetic Materials. *New J. Phys.* **2013**. https://doi.org/10.1088/1367-2630/15/12/125023.

(7) Söderlind, P.; Turchi, P. E. A.; Landa, A.; Lordi, V. Ground-State Properties of Rare-Earth Metals: An Evaluation of Density-Functional Theory. *J. Phys. Condens. Matter* **2014**. https://doi.org/10.1088/0953-8984/26/41/416001.

(8) Landa, A.; Söderlind, P.; Parker, D.; Åberg, D.; Lordi, V.; Perron, A.; Turchi, P. E. A.; Chouhan, R. K.; Paudyal, D.; Lograsso, T. A. Thermodynamics of SmCo5 Compound Doped with Fe and Ni: An Ab Initio Study. *J. Alloys Compd.* **2018**. https://doi.org/10.1016/j.jallcom.2018.06.264.

(9) Landa, A.; Söderlind, P.; Moore, E. E.; Perron, A. Thermodynamics and Magnetism of YCo5 Compound Doped with Fe and Ni: An Ab Initio Study. *Appl. Sci.* **2020**. https://doi.org/10.3390/app10176037.

(10) Arapan, S.; Nieves, P.; Herper, H. C.; Legut, D. Computational Screening of Fe-Ta Hard Magnetic Phases. *Phys. Rev. B* **2020**. https://doi.org/10.1103/PhysRevB.101.014426.

(11) Kovacs, A.; Fischbacher, J.; Gusenbauer, M.; Oezelt, H.; Herper, H. C.; Vekilova, O. Y.; Nieves, P.; Arapan, S.; Schrefl, T. Computational Design of Rare-Earth Reduced Permanent Magnets. *Engineering* **2020**. https://doi.org/10.1016/j.eng.2019.11.006.

(12) Pandey, T.; Du, M. H.; Parker, D. S. Tuning the Magnetic Properties and Structural Stabilities of the 2-17-3 Magnets Sm2Fe17X3 (X= C, N) by Substituting La or Ce for Sm. *Phys. Rev. Appl.* **2018**. https://doi.org/10.1103/PhysRevApplied.9.034002.

(13) Choudhary, R.; Palasyuk, A.; Nlebedim, I. C.; Ott, R. T.; Paudyal, D. Atomic Cooperation in Enhancing Magnetism: (Fe, Cu)-Doped CeCo5. *J. Alloys Compd.* **2020**. https://doi.org/10.1016/j.jallcom.2020.155549.

(14) Xu, K.; Li, H.; Luo, Y.; Wang, L.; Yu, D.; Wang, Z.; Peng, H.; Zhang, Y. Experimental and Computational Study on the Phase Formation and Magnetic Properties of Ce-La-Fe-B Alloys. *J. Magn. Magn. Mater.* **2018**. https://doi.org/10.1016/j.jmmm.2018.04.058.

(15) Martinez-Casado, R.; Dasmahapatra, A.; Sgroi, M. F.; Romero-Muñiz, C.; Herper, H. C.; Vekilova, O. Y.; Ferrari, A. M.; Pullini, D.; Desmarais, J.; Maschio, L. The $CeFe_{11}Ti$ Permanent Magnet: A Closer Look at the Microstructure of the Compound. *J. Phys. Condens. Matter* **2019**, *31* (50), 505505. https://doi.org/10.1088/1361-648X/ab4096.

(16) Dovesi, R.; Orlando, R.; Erba, A.; Zicovich-Wilson, C. M.; Civalleri, B.; Casassa, S.; Maschio, L.; Ferrabone, M.; De La Pierre, M.; D'Arco, P.; Noël, Y.; Causà, M.; Rérat, M.; Kirtman, B. C RYSTAL14: A Program for the Ab Initio Investigation of Crystalline Solids. *Int. J. Quantum Chem.* **2014**. https://doi.org/10.1002/qua.24658.

(17) Locht, I. L. M.; Kvashnin, Y. O.; Rodrigues, D. C. M.; Pereiro, M.; Bergman, A.; Bergqvist, L.; Lichtenstein, A. I.; Katsnelson, M. I.; Delin, A.; Klautau, A. B.; Johansson, B.; Di Marco, I.; Eriksson, O. Standard Model of the Rare Earths Analyzed from the Hubbard i Approximation. *Phys. Rev. B* **2016**. https://doi.org/10.1103/PhysRevB.94.085137.

(18) Ke, L.; Johnson, D. D. Intrinsic Magnetic Properties in R(Fe1-XCox)11TiZ (R= Yand Ce;Z= H,C,and N). *Phys. Rev. B* **2016**. https://doi.org/10.1103/PhysRevB.94.024423.

(19) Yang, Y. chang; Hong, S.; Zhen-yong, Z.; Tong, L.; Jian-liang, G. Crystallographic and Magnetic Properties of Substituted YTi (Fe1-XTx)11. *Solid State Commun.* **1988**.

https://doi.org/10.1016/0038-1098(88)91094-0.

(20) Söderlind, P.; Landa, A.; Locht, I. L. M.; Åberg, D.; Kvashnin, Y.; Pereiro, M.; Däne, M.; Turchi, P. E. A.; Antropov, V. P.; Eriksson, O. Prediction of the New Efficient Permanent Magnet SmCoNiFe3. *Phys. Rev. B* **2017**. https://doi.org/10.1103/PhysRevB.96.100404.

(21) Liu, J.; Moore, J. D.; Skokov, K. P.; Krautz, M.; Löwe, K.; Barcza, A.; Katter, M.; Gutfleisch, O. Exploring La(Fe,Si)13-Based Magnetic Refrigerants towards Application. *Scr. Mater.* **2012**. https://doi.org/10.1016/j.scriptamat.2012.05.039.

(22) Dovesi, R.; Erba, A.; Orlando, R.; Zicovich-Wilson, C. M.; Civalleri, B.; Maschio, L.; Rérat, M.; Casassa, S.; Baima, J.; Salustro, S.; Kirtman, B. Quantum-Mechanical Condensed Matter Simulations with CRYSTAL. *Wiley Interdiscip. Rev. Comput. Mol. Sci.* **2018**. https://doi.org/10.1002/wcms.1360.

(23) Kresse, G.; Hafner, J. Ab Initio Molecular-Dynamics Simulation of the Liquid-Metalamorphous- Semiconductor Transition in Germanium. *Phys. Rev. B* **1994**. https://doi.org/10.1103/PhysRevB.49.14251.

(24) Kresse, G.; Hafner, J. Ab Initio Molecular Dynamics for Liquid Metals. *Phys. Rev. B* **1993**. https://doi.org/10.1103/PhysRevB.47.558.

(25) Kresse, G.; Furthmüller, J. Efficient Iterative Schemes for Ab Initio Total-Energy Calculations Using a Plane-Wave Basis Set. *Phys. Rev. B - Condens. Matter Mater. Phys.* **1996**. https://doi.org/10.1103/PhysRevB.54.11169.

(26) Kresse, G.; Furthmüller, J. Efficiency of Ab-Initio Total Energy Calculations for Metals and Semiconductors Using a Plane-Wave Basis Set. *Comput. Mater. Sci.* **1996**. https://doi.org/10.1016/0927-0256(96)00008-0.

(27) Perdew, J. P.; Burke, K.; Ernzerhof, M. Generalized Gradient Approximation Made Simple. *Phys. Rev. Lett.* **1996**. https://doi.org/10.1103/PhysRevLett.77.3865.

(28) Heyd, J.; Scuseria, G. E.; Ernzerhof, M. Hybrid Functionals Based on a Screened Coulomb Potential. *J. Chem. Phys.* **2003**. https://doi.org/10.1063/1.1564060.

(29) Dasmahapatra, A.; Edith Daga, L.; J. Karttunen, A.; Maschio, L.; Casassa, S. Key Role of Defects in Thermoelectric Performance of TiMSn (M = Ni, Pd, and Pt) Half-Heusler Alloys. *J. Phys. Chem. C* **2020**, *0* (0). https://doi.org/10.1021/acs.jpcc.0c03243.

(30) Shanno, D. F. Conditioning of Quasi-Newton Methods for Function Minimization. *Math. Comput.* **1970**. https://doi.org/10.1090/s0025-5718-1970-0274029-x.

(31) Zicovich-Wilson, C. M.; Dovesi, R. On the Use of Symmetry-Adapted Crystalline Orbitals in SCF-LCAO Periodic Calculations. I. The Construction of the Symmetrized Orbitals. *Int. J. Quantum Chem.* **1998**. https://doi.org/10.1002/(SICI)1097-461X(1998)67:5<299::AID-QUA3>3.0.CO;2-Q.

(32) Maschio, L. Direct Inversion of the Iterative Subspace (DIIS) Convergence Accelerator for Crystalline Solids Employing Gaussian Basis Sets. *Theor. Chem. Acc.* **2018**. https://doi.org/10.1007/s00214-018-2238-8.

(33) Monkhorst, H. J.; Pack, J. D. Special Points for Brillouin-Zone Integrations. *Phys. Rev. B* **1976**. https://doi.org/10.1103/PhysRevB.13.5188.

(34) Daalderop, G. H. O.; Kelly, P. J.; Schuurmans, M. F. H. First-Principles Calculation of the Magnetocrystalline Anisotropy Energy of Iron, Cobalt, and Nickel. *Phys. Rev. B* **1990**. https://doi.org/10.1103/PhysRevB.41.11919.

(35) Wang, X.; Wang, D. S.; Ruqian, W.; Freeman, A. J. Validity of the Force Theorem for

Magnetocrystalline Anisotropy. *J. Magn. Magn. Mater.* **1996**. https://doi.org/10.1016/0304-8853(95)00936-1.

(36) Blöchl, P. E. Projector Augmented-Wave Method. *Phys. Rev. B* **1994**. https://doi.org/10.1103/PhysRevB.50.17953.

(37) Joubert, D. From Ultrasoft Pseudopotentials to the Projector Augmented-Wave Method. *Phys. Rev. B - Condens. Matter Mater. Phys.* **1999**. https://doi.org/10.1103/PhysRevB.59.1758.

(38) Vosko, S. H.; Wilk, L.; Nusair, M. Accurate Spin-Dependent Electron Liquid Correlation Energies for Local Spin Density Calculations: A Critical Analysis. *Can. J. Phys.* **1980**. https://doi.org/10.1139/p80-159.

(39) Mustapha, S.; D'Arco, P.; De La Pierre, M.; Noël, Y.; Ferrabone, M.; Dovesi, R. On the Use of Symmetry in Configurational Analysis for the Simulation of Disordered Solids. *J. Phys. Condens. Matter* **2013**. https://doi.org/10.1088/0953-8984/25/10/105401.

(40) D'Arco, P.; Mustapha, S.; Ferrabone, M.; Noël, Y.; De La Pierre, M.; Dovesi, R. Symmetry and Random Sampling of Symmetry Independent Configurations for the Simulation of Disordered Solids. *J. Phys. Condens. Matter* **2013**. https://doi.org/10.1088/0953-8984/25/35/355401.